University of Huddersfield

University of Huddersfield Repository

Norris, Nicole C, Bingham, Richard, Harris, Gemma, Speakman, Adrian, Jones, Richard P O, Leech, Andrew, Turkenburg, Johan P and Potts, Jennifer R

Structural and functional analysis of the tandem β-zipper interaction of a streptococcal protein with human fibronectin

Original Citation

Norris, Nicole C, Bingham, Richard, Harris, Gemma, Speakman, Adrian, Jones, Richard P O, Leech, Andrew, Turkenburg, Johan P and Potts, Jennifer R (2011) Structural and functional analysis of the tandem β-zipper interaction of a streptococcal protein with human fibronectin. The Journal of biological chemistry, 286 (44). pp. 38311-38320. ISSN 1083-351X

This version is available at http://eprints.hud.ac.uk/id/eprint/11644/

The University Repository is a digital collection of the research output of the University, available on Open Access. Copyright and Moral Rights for the items on this site are retained by the individual author and/or other copyright owners. Users may access full items free of charge; copies of full text items generally can be reproduced, displayed or performed and given to third parties in any format or medium for personal research or study, educational or not-for-profit purposes without prior permission or charge, provided:

- The authors, title and full bibliographic details is credited in any copy;
- A hyperlink and/or URL is included for the original metadata page; and
- The content is not changed in any way.

For more information, including our policy and submission procedure, please contact the Repository Team at: E.mailbox@hud.ac.uk.

http://eprints.hud.ac.uk/

Structural and functional analysis of the tandem β-zipper interaction of a streptococcal protein with human fibronectin

Nicole C. Norris[‡1], Richard J. Bingham[‡2], Gemma Harris[‡], Adrian Speakman[‡], Richard P.O. Jones[‡], Andrew Leech[¶], Johan P. Turkenburg[§], and Jennifer R. Potts[‡§3]

[‡]*Department of Biology,* [¶]*Technology Facility, Department of Biology (Area 15), and* [§]*Department of Chemistry, University of York, York, YO10 5DD, UK*

Running title: Structural and functional analysis of the tandem beta-zipper interaction

[1] *Present address: The John Curtin School of Medical Research, Australian National University, Canberra, Australian Capital Territory, Australia*

[2] *Present address: Department of Chemical and Biological Sciences, School of Applied Sciences, University of Huddersfield, Queensgate, Huddersfield, HD1 3DH, UK*

[3]To whom correspondence should be addressed: Tel.:44-1904-328679; E-mail: jennifer.potts@york.ac.uk

Bacterial fibronectin-binding proteins (FnBPs) contain a large intrinsically-disordered region (IDR) that mediates adhesion of bacteria to host tissues, and invasion of host cells, through binding to fibronectin (Fn). These FnBP IDRs consist of Fn-binding repeats (FnBRs) that form a highly extended tandem β-zipper interaction on binding to the N-terminal domain of Fn. Several FnBR residues are highly conserved across bacterial species, and here we investigate their contribution to the interaction. Mutation of these residues to alanine in SfbI-5 (a disordered FnBR from the human pathogen *Streptococcus pyogenes*) reduced binding but for each residue the change in free energy of binding was <2 kcal/mol. The structure of an SfbI-5 peptide in complex with the second and third F1-modules from Fn confirms that the conserved FnBR residues play equivalent functional roles across bacterial species. Thus, in SfbI-5, the binding energy for the tandem β-zipper interaction with Fn is distributed across the interface rather than concentrated in a small number of "hot spot" residues that are frequently observed in the interactions of folded proteins. We propose that this might be a common feature of the interactions of IDRs, and is likely to pose a challenge for the development of small molecule inhibitors of FnBP-mediated adhesion to and invasion of host cells.

In the last twenty years there has been increasing recognition of the functional importance of regions of protein sequence that lack a stable tertiary fold under physiological conditions (1,2). Previously the "structure-function paradigm" asserted that a protein must be stably folded to be functional. However it has since been shown that intrinsically disordered regions (IDRs) are involved in key molecular recognition events in both physiological (3) and pathological processes (4) and that IDRs often become structured on binding (5).

Our previous work has shown that cell-wall attached proteins expressed by some staphylococci and streptococci species and also the Lyme disease-causing spirochete, *Borrelia burgdorferi*, contain IDRs which bind the protein fibronectin (Fn) through a highly unusual mechanism of protein-protein recognition which we called a tandem β-zipper (6-11). This work investigates the thermodynamics of this interaction by studying the binding of Fn to SfbI, a Fn-binding protein (FnBP) from *Streptococcus pyogenes*.

Fn is a chordate glycoprotein (12). It is found as a disulfide-linked dimer in human plasma and in an insoluble fibrillar form as a component of extracellular matrices. Fn plays an essential role in development (13,14) and in other processes requiring cell migration, such as wound healing and tissue remodeling (15). Fn is a modular protein and the N-terminal domain (NTD) contains a string of five Fn type I (F1) modules ($^{1-5}$F1) whose sequences are highly conserved across vertebrates (16). IDRs within bacterial FnBPs interact with these F1 modules.

S. pyogenes is an important human pathogen that causes common infections of the throat and skin such as pharyngitis and impetigo, and can also cause more severe invasive infections such as streptococcal toxic shock syndrome and necrotizing fasciitis (reviewed in (17)). SfbI mediates bacterial invasion of epithelial cells and endothelial cells (18-20) by binding to Fn, which acts as a bridge between SfbI and host cell

integrins. Internalization might allow *S. pyogenes* to avoid anti-microbial drugs and host-defense mechanisms (reviewed in (21) and (22)) and, thus, is a potential target for new therapeutics.

Biophysical studies have shown that an FnBP from *Staphylococcus aureus* contains a series of intrinsically disordered Fn-binding repeats (FnBRs) that undergo a disorder-to-order transition on binding either $^{2-4}$F1 or $^{2-5}$F1 from the NTD of Fn (10,23,24). In this tandem β-zipper interaction, the FnBR extends the triple-stranded anti-parallel β-sheet of sequential F1 modules by forming an additional strand anti-parallel to the C-terminal strand (strand E) of each F1 module (7,25). SfbI from *S. pyogenes* contains five FnBRs that each bind the NTD of Fn (7,8,22). SfbI-5, the most C-terminal FnBR also has a ^{1}F1-binding motif and can, therefore, bind all five F1 modules ($^{1-5}$F1). To date, ^{1}F1-binding motifs have only been identified in C-terminal streptococcal FnBRs (7,22).

The thermodynamics of protein-protein interactions involving two folded proteins have been well-studied. Mutational analyses show that the free-energy of binding is often concentrated within a few hot spot residues (26) (change in Gibbs free energy of binding, $\Delta\Delta G°$, on mutation of >2 kcal/mol) rather than being distributed evenly across the interface (27). The ability to identify hot spot residues is particularly important for the discovery of drugs that target protein-protein interactions (28) and there are now a number of web servers that will perform such predictions (29-31). Much less is known about the thermodynamics of the interactions of IDRs.

In this study we demonstrate that SfbI-5 is an IDR. We use a Hidden Markov Model (HMM) to identify the most conserved FnBR residues across bacterial species. We show that for the NTD:SfbI-5 tandem β-zipper interaction, residues that are highly conserved across FnBRs, and that form very similar intermolecular interactions in NTD:FnBR complexes across bacterial species, are not hot spot residues. Therefore, unlike many interfaces formed between folded proteins, for SfbI-5 the binding energy is distributed across the interface. We suggest this might be a feature of the rather extended interactions that many IDRs form relative to folded proteins (32). The distributed energy of binding will pose a challenge to the development of small molecules that inhibit FnBP-mediated adhesion to and invasion of host cells.

EXPERIMENTAL PROCEDURES

Proteins, Proteolytic fragments, Synthetic Peptides, Protein Expression and Purification – The synthetic peptide PyTT5, corresponding to residues 560–577 of SfbI (UniProt accession Q01924), was purchased from Alta Bioscience (Birmingham, UK). The N- and C-termini were capped by acetylation and amidation, respectively. Human plasma Fn was purchased from Sigma Aldrich (product no. F0895). The N-terminal domain from human plasma Fn, containing $^{1-5}$F1, was purchased as a 30 kDa proteolytic fragment from Sigma Aldrich (product no. F9911) and is referred to as pNTD herein. The N- and C-termini were determined by mass spectrometry (MS) using an *apex ultra* FTMS (Bruker Daltonics).

^{2}F1^{3}F1 (residues 62–151 of mature human Fn) was expressed in *Pichia pastoris* and purified using procedures similar to those described previously (7,33). SfbI-5 (corresponding to residues 542–591 of SfbI) was expressed as a recombinant glutathione *S*-transferase (GST) fusion using the pGEX-5X-SfbI-5 construct described previously (7). *Escherichia coli* BL21 Gold competent cells (Stratagene) were transformed with pGEX-5X-SfbI-5 using a rapid protocol (34). A culture of a single transformed colony inoculated into LB-Amp broth (1% (w/v) tryptone, 0.5% (w/v) yeast extract, 1% NaCl (w/v), 100 µg/ml ampicillin) was grown for ~18 h at 37°C and then diluted into LB-Amp broth and incubated with shaking at either 30°C or 37°C. Cultures were induced to over-express the GST fusion with isopropyl β-*D*-thiogalactopyranoside when the optical density at 600 nm was between 0.6 and 1.2, and were then grown for a further 17 h (30°C) or 3 h (37°C). The GST fusion protein was purified from cleared cell lysates using glutathione Sepharose (GE Healthcare).

For ITC and NMR experiments, SfbI-5 was cleaved from GST with Factor Xa (New England Biolabs), purified by reversed-phase high performance liquid chromatography (8) and lyophilized. The mass of the purified product was confirmed by MS. ^{15}N, ^{13}C-labelled SfbI-5 was produced using similar methods but using isotope-labelled minimal media.

Site-directed Mutagenesis – All SfbI-5 mutants were created through site-directed mutagenesis of pGEX-5X-SfbI-5 using the

Quikchange II mutagenesis kit (Stratagene), and the primers in Supplemental Table 1. In-house DNA sequencing confirmed the presence of mutations. SfbI-5 mutants were expressed, purified and lyophilized as for wild type SfbI-5, and their masses confirmed by MS.

Isothermal Titration Calorimetry (ITC) – The binding of pNTD to SfbI-5 and SfbI-5 mutants was measured in PBS (140 mM NaCl, 2.7 mM KCl, 10 mM Na_2PO_4, 1.8 mM KH_2PO_4) at 37°C using a VP-ITC microcalorimeter (MicroCal) and a procedure very similar to that reported previously (8). For each SfbI-5 peptide, an ITC experiment consisted of a binding titration and a control titration; the SfbI-5 peptide titrated into PBS with or without pNTD, respectively. The experiments were performed with pNTD (1.4–4 μM) in the cell and the peptide (20–50 μM) in the syringe. The experiments with the following SfbI-5 peptides were performed twice: SfbI-5, F554A, K556A, K556E, D574A and T575A; and those with T558A were performed three times. Data were analyzed and fitted to a single site binding model using non-linear regression analysis in Origin 7.0 software (MicroCal).

The concentration of pNTD was determined by absorbance at 280 nm using a theoretical extinction coefficient, based on the amino acid sequence, of 63130 M^{-1} cm^{-1}. The concentration of the SfbI-5 peptide was initially estimated from the weight of lyophilized material and then determined for one syringe sample for the following SfbI-5 peptides by quantitative amino acid analysis (Alta Bioscience, Birmingham): SfbI-5, F554A, K556A, K556E, T558A, and D574A. Use of these peptide concentrations resulted in molar ratio of binding (*n*) values within 12% of 1.0. Thus, for all other titrations, the peptide concentrations were corrected during analysis to give an *n* value of 1. Heats of dilution were either the injection of the appropriate peptide into buffer or the average peak area of the last five or ten injections from the binding titration. For those SfbI-5 mutants whose ITC experiments were repeated, the mean value of each parameter was used for subsequent analysis.

NMR Spectroscopy – A standard suite of triple-resonance experiments was performed for sequential assignment of ^{15}N, ^{13}C-labelled SfbI-5 (1 mM, pH 5.5, 10% (v/v) D_2O, 0.02% (w/v) NaN_3). All were acquired using standard Bruker pulse sequences on a Bruker AVII 700 MHz spectrometer equipped with a triple resonance (HCN) probe and z-axis gradients at 25°C. Data were processed using NMRPipe (35) and analyzed using CCPN Analysis (36).

Secondary structure propensity (SSP) was calculated from the assigned chemical shifts of the SfbI-5 $^{1}H^{N}$, $^{15}N^{H}$, $^{13}C^{\alpha}$, $^{13}C^{\beta}$ and $^{13}C'$ nuclei (Supplemental Table 2) using the SSP Perl script kindly made available for download by Marsh *et al.* (37). The input used for the script was the experimentally-determined SfbI-5 chemical shifts and the statistically-derived random coil dataset from Wang and Jardetzky (38). Appropriate sequence correction values for the random coil dataset (38) were added to the corresponding observed SfbI-5 chemical shifts before SSP score calculation.

X-ray Crystallography – Crystals of $^{2}F1^{3}F1$:PyTT5 (0.3 mM/~3.5 mM, pH 7.7) were grown using sitting drop vapour diffusion from a 1:1 dilution with the well solution. The well solution was either 20 mM $MgCl_2$, 0.1 M HEPES pH 7.5, 22% w/v polyacrylic acid or 0.1 M Tris pH 7.0, 1.5 M $(NH_4)_2SO_4$ for the lower and higher resolution data, respectively. Crystals were flash-cooled in liquid nitrogen using 20% or 30% (v/v) glycerol as the cryoprotectant.

Data Collection and Refinement – The lower resolution data were collected in-house at 120 K and the higher resolution data at 100 K at the European Synchrotron Radiation Facility on the ID23-1 beamline. Statistics are provided in Supplemental Table 3. Data were processed and scaled using MOSFLM/SCALA (39-41). Successful solution of the lower resolution data was obtained by molecular replacement using models of $^{2}F1$ and $^{3}F1$ (pdb code 2RKZ) (25), searched for separately within Phaser (42). This structure was refined as described previously (25) and was used (without PyTT5) as the starting point for refinement of the higher resolution data using REFMAC (43).

Creation of Hidden Markov Model – A profile HMM (44) was assembled using the sequences of known FnBRs (22) and using structural data (25) to inform where gaps in the alignment would be more likely. The HMM was used to search for other FnBRs in the UniRef90 sequence database (45). A set of non-redundant FnBRs was created from those identified in the search, in which each FnBR had no more than 70% pairwise identity to any other FnBR in the set. An HMM representing the non-redundant FnBRs was used in a second search of the database. This iterative process was repeated three times, until no further FnBRs were identified. An HMM logo was produced (46)

using a final HMM of all non-identical FnBRs.

Model of $^{1-5}$F1:SfbI-5 – The model of $^{1-5}$F1:SfbI-5 was built from the structure of ^{2}F1^{3}F1:PyTT5, an alignment between ^{4}F1^{5}F1 and *S. aureus* FnBPA peptide structures (pdb codes 2RKY and 2RL0) (25), and ^{1}F1 and the ^{1}F1-binding region from the structure of ^{1}F1^{2}F1 in complex with B3T (pdb code 1O9A) (7) using the program Modeller (47). The ^{1}F1^{2}F1 interface is not well-defined even in the presence of peptide (7).

Surface Plasmon Resonance (SPR) – Interactions of SfbI-5 with human Fn and pNTD were studied using SPR. Binding studies were performed using a BIAcore T100 instrument (GE Healthcare) at 25°C. GST-tagged wild-type or mutant (T558A) SfbI-5 was immobilized onto the experimental flow cell of a certified C1 sensor chip (GE Healthcare) by amine coupling using N-hydroxysuccinimide (NHS) and ethyl (dimethylaminopropyl) carbodiimide (EDC). Ethanolamine was subsequently used to block the surface. The reference flow cell underwent an identical but blank immobilization and blocking protocol. The SPR running buffer was HBSP (10 mM HEPES pH 7.4, 150 mM NaCl, 0.05% (v/v) polysorbate 20). Flow rates of 20 µl/min and 30 µl/min were used for data acquisition and regeneration, respectively. The analyte contact and dissociation times were 180 s and 600 s or 1200 s, respectively. The longer dissociation time was required for the interaction of wild-type SfbI-5 with Fn, to ensure dissociation of a significant amount of analyte from the ligand. Regeneration contact and stabilization times were 540 s and 3000 s, respectively. 0.1 M NaOH was used for regeneration. A kinetic data series contained sensorgrams measured for seven or eight sequential two-fold analyte dilutions from 13.9 nM for both Fn and pNTD. Kinetic data series were fitted to a Langmuir 1:1 binding model by Biacore T100 Evaluation Software (GE Healthcare) using a constant, zero bulk refractive index parameter. An upper limit for analyte concentration for sensorgram analysis was determined to ensure reliable curve-fitting indicated by low χ^2 values. For the interaction between pNTD and SfbI-5 T558A, steady state affinity analysis was used to determine the binding affinity by Biacore T100 Evaluation Software (GE Healthcare) using a constant zero offset.

RESULTS

SfbI-5 is an IDR – SfbI-5 binds to pNTD with the highest affinity (K_d ~3nM at 37°C) (8) of the FnBRs studied to date. Although SfbI-5 is predicted to be an IDR based on its sequence, this has not been confirmed experimentally. In the absence of pNTD, the ^{15}N-^{1}H HSQC NMR spectrum of ^{15}N, ^{13}C-labelled SfbI-5 has the narrow line-widths and low chemical shift dispersion in the ^{1}H dimension typical of an IDR (Fig. 1*A*). To confirm this observation, standard NMR methods were used to assign chemical shifts to the $^{1}H^{N}$, $^{15}N^{H}$, $^{13}C^{\alpha}$, $^{13}C^{\beta}$ and $^{13}C'$ nuclei (Supplemental Table 2). The secondary structure propensity for each residue was determined by calculation of its SSP score, using the assigned chemical shifts and those predicted for a sequence-corrected random coil (37,38) (Fig. 1*B*).

No evidence of stable secondary structure, nor significant SSP, was detected in the $^{2-5}$F1 binding region of SfbI-5. This is consistent with previous circular dichroism results that streptococcal and staphylococcal FnBRs are IDRs (48), and also with a previous NMR analysis of an FnBR-containing region in *S. aureus* FnBPA (6). However, unlike other FnBRs in SfbI, SfbI-5 contains a ^{1}F1-binding region (residues 577–588) (7) and this region has SSP for β-strand conformations (Fig. 1*B*). In particular, residues 580–584 have an SSP score of less than −0.3, indicating that within this region more than a third of the SfbI-5 molecules exhibit φ and ψ angles typical of β-strand at any given time. This provides a plausible explanation for our previous observation that the ^{1}F1^{2}F1-binding motif from SfbI-5 bound with higher affinity than SfbI peptides that bind ^{2}F1^{3}F1 or ^{4}F1^{5}F1 (8).

Conservation of FnBR residues – Fig. 2 shows an HMM logo (46) assembled from an alignment of all non-redundant staphylococcal, streptococcal and spirochetal FnBRs identified in the sequence databases. Fig. 2 shows that, particularly in the FnBR region that binds ^{2}F1^{3}F1, there are residues that are highly conserved across all FnBRs.

Effect of Mutation of Conserved FnBR Residues on Affinity of the Interaction of SfbI-5 with $^{1-5}$F1 – The effect of mutating conserved SfbI-5 residues on the binding of SfbI-5 to $^{1-5}$F1 was investigated using ITC. The ^{2}F1- and ^{4}F1-binding regions contain the most conserved FnBR residues (Fig. 2). Additionally, we have previously shown that, of the $^{2-5}$F1-binding

regions, only the ^{2}F1- and ^{4}F1-binding regions show significant binding to F1 module pairs that contain their target F1 module (8). Thus, we focused the mutation analysis on these regions and on the highly conserved Gly in the ^{3}F1-binding region. Also, for comparison, we mutated two residues with lower levels of conservation; one in the ^{2}F1- and one in the ^{3}F1-binding region.

As can be observed from Table 1 and Fig. 3, when conserved residues in SfbI-5 were mutated to alanine, the binding became weaker relative to wild-type SfbI-5. In the one case where a residue in SfbI-5 that was not the consensus FnBR residue for that position (Fig. 2) was mutated to the consensus residue (K556E), the binding was significantly tighter relative to wild-type SfbI-5. Thus, overall, these results are consistent with the HMM logo in Fig. 2. However, while mutation of all the conserved residues weakened the interaction, for even the most conserved FnBR residues, the effect of mutation was relatively modest when compared with the effect of mutating hot spot residues on the interactions of folded proteins (defined here as those that contribute more than 2 kcal/mol to the interaction (26)).

Key interactions are conserved between S. aureus FnBPA and S. pyogenes SfbI in binding to ^{2}F1^{3}F1 – To test whether residues conserved across FnBRs play the same functional role in the binding of different organisms to Fn, we determined the structure of ^{2}F1^{3}F1 in complex with PyTT5 (the ^{2}F1^{3}F1-binding peptide from SfbI-5) and compared it to our previously determined structures of homologous peptides from *S. aureus* FnBPA in complex with ^{2}F1^{3}F1 (^{2}F1^{3}F1:STATT1 and ^{2}F1^{3}F1:STATT5; pdb codes 2RKZ and 3CAL, respectively (25)).

Fig. 4 shows the 1.7 Å resolution structure of PyTT5 in complex with ^{2}F1^{3}F1 (crystallographic parameters are provided in Supplemental Table 3). It is clear that PyTT5 binds the E strands of ^{2}F1 and ^{3}F1 through a tandem β-zipper mechanism (Fig. 4*A*), with PyTT5 residues 562–565 and 570–574 adopting φ and ψ angles typical of β-strand. As expected, there is little difference in the F1 module structures; comparison of the structure with that of ^{2}F1^{3}F1:STATT1 shows a root mean squared deviation of 2.11 Å between ^{2}F1^{3}F1 in the two structures.

The side-chains of the PyTT5 ^{3}F1-binding region (residues 560–565) interact with ^{3}F1 primarily *via* van der Waals contacts, with M562 contacting L134 and R125 in ^{3}F1, and F565 stacking against aliphatic side-chain atoms of K143 and E145 (Fig. 4*C*). Furthermore, a glycine at position 564 allows PyTT5 to adopt a β-strand conformation without a steric clash with W146 in ^{3}F1 (Fig. 4*C*). Thus, the highly conserved glycine identified in Fig. 2 performs the same function in this structure as in the two structures of ^{2}F1^{3}F1 with *S. aureus* peptides (25).

The PyTT5 linker region (residues 566–569) does not loop away from ^{2}F1^{3}F1 as in the ^{2}F1^{3}F1:STATT1 and ^{2}F1^{3}F1:STATT5 structures (25), although it is the same length as the linker region in STATT5 (25). Instead, the PyTT5 linker binds to the interface between ^{2}F1 and ^{3}F1 primarily *via* hydrogen bonds; the side-chains of bacterial residues S566 and E567 participate in hydrogen bond networks involving residues in both ^{2}F1 and ^{3}F1 (Fig. 4*C*).

The PyTT5 ^{2}F1-binding region (residues 570–577) binds to ^{2}F1 *via* both van der Waals and hydrogen bond interactions. The two key van der Waals contacts are between the side-chains of the bacterial residues I571 and D574 and the side-chains of W90 and R99 of ^{2}F1, respectively. T570 forms a hydrogen bond with the side-chain of T105 in ^{2}F1, adopting a staggered conformation favoured in β-sheets (49). The side-chain of E573 exists in two conformations in both ^{2}F1^{3}F1:PyTT5 complexes in the asymmetric unit with approximately 50% occupancy in each conformation. One of the conformations results in a salt bridge to the side-chain of R83 in ^{2}F1 (Fig. 4*D*) as found for the corresponding side-chain in both complexes of *S. aureus* peptides with ^{2}F1^{3}F1 (25). The second E573 side-chain conformation forms a hydrogen bond to the carbonyl group of D574 *via* a bridging water molecule (Fig. 4*D*). The side-chain of D574 forms a salt bridge with both R101 and R99, and T575 forms hydrogen bonds to the backbone atoms of G100 and F67, although the latter is *via* a bridging water molecule (Fig. 4*D*). Therefore, the PyTT5 residues corresponding to the conserved 'E-(D/E)-(T/S)' motif identified in Fig. 2 form interactions in the complex that are very similar to those of the corresponding residues in the ^{2}F1^{3}F1:STATT1 and ^{2}F1^{3}F1:STATT5 complexes (25).

PyTT5 efficiently forms an extended interface with ^{2}F1^{3}F1 – The extent of the interface between PyTT5 and ^{2}F1^{3}F1 was analysed using

ProFace (50). A protein interface can be divided into two categories at both the atom and residue level (51,52). At the atom level, the interface can be divided into buried and accessible interface atoms, where buried atoms lose all accessible surface area (ASA) on complex formation and accessible atoms lose some ASA. The ProFace analysis showed that every residue of PyTT5 is involved in the interface with ^{2}F1^{3}F1, with at least one atom of each residue in PyTT5 having some buried surface area at the interface (Fig. 5*A*; Table 2).

At the residue level, the interface can be divided into core and rim residues, with core residues containing at least one buried interface atom and rim residues containing at least one accessible interface atom and no buried interface atoms. By this definition, 14 of the 18 residues (78%) in PyTT5 were core residues and the remaining residues were rim residues (32%). In comparison, ^{2}F1^{3}F1 had 20 core residues (22%) and 18 rim residues (20%) out of a total of 89 residues (Table 2). This indicates that each residue of PyTT5 contacts, on average, more residues of ^{2}F1^{3}F1 than *vice versa*. It also indicates that a much greater percentage of PyTT5 is involved in the interface compared to ^{2}F1^{3}F1. This is further shown by the fact that 40% of the ASA of PyTT5 is buried at the interface, compared to 17% of the ASA of ^{2}F1^{3}F1. Thus, PyTT5 is a very efficient ligand. These properties have been noted in other complexes involving IDRs (32,53,54).

SfbI-5 is Predicted to Form a Large, Extended Interface with $^{1-5}$F1 – Structural data is now available for a single ^{1}F1^{2}F1:FnBR peptide complex (7), three ^{2}F1^{3}F1:FnBR (25) peptide complexes and two ^{4}F1^{5}F1:FnBR peptide complexes (25), so it is intriguing to consider the extent of the interface between SfbI-5 and $^{1-5}$F1. ProFace analysis of a model of $^{1-5}$F1 bound to SfbI-5 (Fig. 6) predicts that the total buried surface area of the interface would be ~5150 Å^{2}. This is a very large interface for a heterocomplex. In fact, comparison between the predicted interface area of $^{1-5}$F1:SfbI-5 and the observed interface areas from a set of heterodimer complex structures from the Protein Data Bank (32) reveals that the predicted interface is larger than any of the interfaces in the dataset, and more than 1500 Å^{2} larger than the largest complex involving an IDR.

Furthermore, 40% of the ASA of SfbI-5 is buried in the interface, compared to 18% of the ASA of $^{1-5}$F1. Thus, the reasons PyTT5 is an efficient ligand for binding to ^{2}F1^{3}F1 are also predicted to make SfbI-5 an efficient ligand when in complex with $^{1-5}$F1. For a globular protein to bury a similar amount of surface area it would have to have two to three times more residues. Therefore, a probable biological advantage of the intrinsic disorder of SfbI-5 is large interface formation (and tight binding) with fewer resources committed on the part of *S. pyogenes* (53).

Effect of Mutation of Conserved FnBR Residues on Affinity of the Interaction of SfbI-5 with Fn – In vivo, SfbI-5 interacts with $^{1-5}$F1 in the context of intact Fn. Thus, the effect of the mutation of conserved FnBR residues on binding to plasma Fn was also determined (Fig. 7). SPR was first used to determine the dissociation constants for binding to pNTD (to compare with values obtained using ITC). The results were remarkably similar, with the T558A mutation causing a 19-fold reduction in the affinity when measured using SPR (Table 3) compared with a 16-fold reduction in affinity when measured using ITC (Table 1). When binding of Fn to wild-type SfbI-5 and the T558A mutant were compared, the mutation resulted in an approximately five-fold reduction in the affinity. Thus, the T558A mutation has an even smaller effect on binding to Fn.

DISCUSSION

SfbI-5 is an IDR – Comparison of the chemical shifts of the SfbI-5 ^{1}H^{N}, ^{15}N^{H}, ^{13}C$^{\alpha}$, ^{13}C$^{\beta}$ and ^{13}C′ nuclei with sequence-corrected random coil values revealed that SfbI-5 is an IDR, with no evidence of any stable secondary structure. However, the C-terminal ^{1}F1-binding region of SfbI-5 showed significant propensity for β-strand formation. Based on a sequence alignment between SfbI-5 and the *S. dysgalactiae* FnBR peptide B3T, whose structure has been solved in complex with ^{1}F1^{2}F1 (7), the residues with high β-strand propensity are predicted to form a β-strand when bound to ^{1}F1. Therefore, this region might be a preformed structural element primed for ^{1}F1 recognition (55).

Conserved Residues in Streptococcal and Staphylococcal FnBRs Perform Similar Functions – The crystal structure of PyTT5 in complex with ^{2}F1^{3}F1 shows that the peptide binds to ^{2}F1^{3}F1 *via* a tandem β-zipper (Fig. 4*A*). Comparison of this structure to those of FnBPA peptides in complex with ^{2}F1^{3}F1 (25) revealed

that residues that were conserved between these peptides formed similar interactions with ^{2}F1^{3}F1. Given the sequence similarity between the other F1-binding regions of SfbI with FnBR peptides that have been solved in complex with ^{4}F1^{5}F1 and ^{1}F1^{2}F1 (7,23,25), it is highly likely that SfbI-5 will bind to ^{1}F1 and ^{4}F1^{5}F1 *via* a tandem β-zipper. Thus, we prepared a model of the intact complex that highlights the extraordinary efficiency of the interaction (Fig. 6).

High efficiency of extended interface formation has been proposed as a potential advantage of intrinsic disorder (53) and overall, interface area per IDR residue is higher in protein-protein heterocomplexes containing an IDR than for complexes containing two folded proteins (32). The tandem β-zipper interaction of SfbI-5 with $^{1-5}$F1 provides a clear demonstration of the efficiency of extended interface formation and the high affinity that can be achieved by an IDR. As seen previously for FnBR peptide interactions with F1 modules, there is little change in the ^{2}F1^{3}F1 structure on PyTT5-binding.

Analysis of ΔΔG° values – The effect of mutating conserved SfbI-5 residues on the binding of SfbI-5 to pNTD was determined by calculating the ΔΔG° for binding of the SfbI-5 mutants relative to wild-type SfbI-5 (Table 1). Most of the effects of the mutations can be rationalized from the structures based on the loss of buried atoms or intermolecular hydrogen bonds involving the mutated residue.

Some of the effects of mutations could also have been predicted based on residue conservation (Fig. 2). For example, K556A had a small but favourable ΔΔG° of −0.47 kcal/mol and K556E had a more favourable ΔΔG° of −0.90 kcal/mol. This result would be predicted from Fig. 2 as glutamate is the most conserved residue at this position. Also, for G564A, the unfavourable change in free energy is likely caused by changes in surrounding interactions that are required to avoid a steric clash between the alanine side-chain and the W146 of ^{3}F1 (Fig. 4*C*).

However, a comparison of Table 1 and Fig. 2 shows that overall there is not a strong correlation between the level of conservation of a residue and the ΔΔG° value for mutation of that residue. The largest effect is observed for T558A, yet T558 is not, by some way, the most highly conserved residue. I571 and M562 were mutated because they are less well conserved (Fig. 2) and were predicted to form β-strand interactions with an F1 module primarily *via* backbone-backbone hydrogen bonds, a prediction that was confirmed by the ^{2}F1^{3}F1:PyTT5 structure (Fig. 4*C*, *D*). Yet the small ΔΔG° values (0.49 and 0.53 kcal/mol, respectively) for mutation for these residues are similar to that observed for the mutation of a highly conserved acidic residue (E553) in the conserved 'E-(D/E)-(T/S)' motif within the ^{2}F1-binding region.

The energy of the NTD:SfbI-5interaction is distributed across the interface – All mutations of conserved residues reduced the affinity of binding, but ΔΔG° values were relatively small (less than 2.0 kcal/mol) compared to similar analyses on mutating interfaces in globular complexes (56,57). Some analyses use a different threshold (e.g. ΔΔG° >1 kcal/mol (31)) for defining hot spot residues. The latter threshold would mean that four SfbI-5 residues were hot spots (F554, T558, G564 D574). Interestingly, only one of these residues is from the ^{2}F1-binding region, yet it is this region that binds more tightly to ^{2}F1^{3}F1 (8). However, regardless of the threshold chosen, it is clear from Table 1 that in the NTD:SfbI-5 interaction, the binding energy is distributed across the large interface rather than being concentrated in a few residues.

It has been observed that hot spots tend to be core residues, and tend not to be rim residues. This is because core residues form side-chain interactions with the protein partner and rim residues act like an 'o-ring' and shield the core residues from water (58). However, the extended nature of PyTT5, when in complex with ^{2}F1^{3}F1, means that PyTT5 does not contain an 'o-ring' of rim residues (Fig. 5*B*). Based on our model (Fig 6), intact SfbI-5, when in complex with $^{1-5}$F1, would also lack o-ring residues. The reason this might lead to the absence of hot spots can be better understood by considering the interface at the level of atoms.

At the atom level of protein-protein interactions, the main-chain is not directly affected by site-directed mutagenesis to alanine (51). Also, when accessible interface atoms are removed by mutation, they can be replaced by water molecules at a lower energetic cost than buried atoms (51). By this rationale, hot spot residues are likely to contain a buried interface atom that is deleted when the residue is mutated to alanine. Only two of 22 (9.1%) buried interface atoms in PyTT5 but 14 of 44 (32%) in ^{2}F1^{3}F1 fulfill these criteria. Therefore, it appears

the extended nature of the interface between SfbI-5 and $^{1-5}$F1, which is facilitated by the intrinsic disorder of free SfbI-5, is likely to preclude the presence of hot spot residues in SfbI-5. A more even distribution of the free energy of binding might be a more general property of complexes containing IDRs that have extended interfaces (32) which are unlikely to shield important interacting residues from water.

We used the HotPOINT server (59) to analyse ^{2}F1^{3}F1:PyTT5, and *S. aureus* FnBR peptides in complex with ^{2}F1^{3}F1 (2RKZ and 3CAL) and ^{4}F1^{5}F1 (2RKY and 2RL0) (25) to predict hot spots. Consistent with our ITC results, this analysis also suggests an overall lack of hot spots in the FnBR peptides with only a single conserved residue in the FnBR peptides (and only in 2RL0) predicted to be a hot spot.

A paradox and a challenge – We have shown that conserved residues in FnBRs of *S. pyogenes* and *S. aureus* play equivalent functional roles in binding to Fn and that single interactions can be sacrificed (*in vitro*) whilst maintaining a high affinity interaction. But why then are the FnBR residues so conserved? That is, are the conserved residues important for an aspect not probed by our pNTD-interaction assay, or are the small changes in affinity observed functionally significant?

Other potential functional roles for the conserved residues that are not probed by the pNTD-binding assay are the disruption of intramolecular Fn interactions and/or maintenance of disorder in the FnBR. Long-range intra-molecular interactions between $^{2-5}$F1 and Fn type 3 modules (60) have recently been shown to mask motogenic sites within the collagen-binding domain of Fn. Changes in chemical shifts in the N-terminal strand (A strand) and E strands of F1 modules on F3 module binding (60) suggests that the F3 and SfbI-5 binding sites on $^{2-5}$F1 partially overlap. The faster association rate observed for binding of wild-type SfbI-5 to pNTD compared to Fn (Table 3) is consistent with the FnBR binding site being somewhat cryptic in Fn. Therefore, we reasoned that conserved residues might play a role in unmasking the binding site and, thus, the effect of their mutation would only be observed when binding to Fn (rather than pNTD) was measured. However, the mutation that had the largest effect on SfbI-5 binding to pNTD (T558A) had an even smaller effect on the K_d for binding to intact Fn, suggesting that the interaction with Fn also lacks hot spots in the IDR.

Conserved residues might also play a role in maintaining the disordered state of FnBRs, similar to conservation of structurally important residues in a folded protein. By definition, disordered proteins do not make enough energetically favourable intramolecular contacts to overcome the unfavourable entropy of folding into a stable tertiary structure. This is achieved by a characteristic amino acid composition, with IDRs having on average more charged and polar residues and fewer hydrophobic residues (61). It also requires each residue to limit the number of favourable interactions it makes with its neighbouring residues (62). Therefore, there might be selective pressure for a disorder-promoting residue at a given position in an IDR depending on its neighbouring sequence. Whether this selective pressure exists in FnBRs is hard to identify given current knowledge of IDR residue conservation.

Only streptococcal FnBPs, and in each case, only the C-terminal FnBR in the protein, contains a ^{1}F1-binding motif. These $^{1-5}$F1 binding FnBRs bind NTD with higher affinity than $^{2-5}$F1-binding FnBRs in SfbI (8). For example, in our previous study SfbI-5 bound pNTD with a K_d of ~2 nM at 37°C, while SfbI-4 bound with a K_d of 60 nM at 25°C (8). While *S. aureus* FnBPs only contain $^{2-5}$F1-binding FnBRs, the C-terminal FnBR (FnBPA-11) also binds NTD with the highest affinity; K_d <1 nM at 25°C compared to 5 nM for FnBPA-1 (10). Thus, selective pressure for the maintenance of high affinity binding at the most C-terminal FnBR might operate *in vivo*, for example, at the level of integrin-mediated bacterial invasion.

The extended, multi-domain nature of the tandem β-zipper interface is a plausible (and intuitive) explanation for the apparent absence of hot spots in SfbI-5. The mutation analysis of the NTD:SfbI-5 interaction presented here provides experimental support for this intuition. This interaction is, as yet, unusual with the only other reported example in LIM/Ldb interactions (54). However, extended interactions appear to be favoured by IDRs (32), and, thus, we suggest that IDRs in general might be more likely to form interactions that lack well-defined hot spots.

Rational design strategies for drugs that target protein-protein interactions are still in the relatively early stages of development (28). The additional challenges involved in the design of

drugs that target interactions involving IDRs has recently been highlighted (63). The more even distribution of binding energy over the interface, as observed here, than is commonly observed in the binding of folded proteins, will add a further challenge; specifically for development of inhibitors of FnBP-mediated invasion of host cells and perhaps more generally for interactions involving IDRs.

*This work was supported by a British Heart Foundation Senior Basic Science Fellowship (to JRP), an Overseas Research Students Awards Scheme Scholarship and scholarships from the Universities of Sydney and York (to NN) and by the Biotechnology and Biological Sciences Research Council (grant D010608/1). Adam Dowle is thanked for the mass spectrometry of $^{1-5}$F1, Sam Hart for X-ray data collection, Peter Ashton for assistance with bioinformatics and David Williamson and Andrew Brentnall for assistance with the acquisition and processing of the NMR spectra. We thank the ESRF, Grenoble, for excellent data collection facilities.
The atomic coordinates have been deposited in the Protein Data Bank (pdb code 3zrz).

REFERENCES

1. Dunker, AK, Brown, CJ, Lawson, JD, Iakoucheva, LM, & Obradović, Z. (2002) *Biochemistry* **41**, 6573-6582
2. Tompa, P. (2005) *FEBS Lett.* **579**, 3346-3354
3. Liu, J, Perumal, NB, Oldfield, CJ, Su, EW, Uversky, VN, & Dunker, AK. (2008) *Biochemistry* **45**, 6873-6888
4. Uversky, VN, Oldfield, CJ, & Dunker, AK. (2008) *Ann. Rev. Biophys.* **37**, 215-246
5. Dyson, HJ, & Wright, PE. (2002) *Curr. Opin. Struct. Biol.* **12**, 54-60
6. Penkett, CJ, Redfield, C, Jones, JA, Dodd, I, Hubbard, J, Smith, RAG, Smith, LJ, & Dobson, CM. (1998) *Biochemistry* **37**, 17054-17067
7. Schwarz-Linek, U, Werner, JM, Pickford, AR, Gurusiddappa, S, Kim, JH, Pilka, ES, Briggs, JA, Gough, TS, Höök, M, Campbell, ID, & Potts, JR. (2003) *Nature* **423**, 177-181
8. Schwarz-Linek, U, Pilka, ES, Pickford, AR, Kim, JH, Höök, M, Campbell, ID, & Potts, JR. (2004) *J. Biol. Chem.* **279**, 39017-39025
9. Raibaud, S, Schwarz-Linek, U, Kim, JH, Jenkins, HT, Baines, ER, Gurusidappa, S, Höök, M, & Potts, JR. (2005) *J. Biol. Chem.* **280**, 18803-18809
10. Meenan, NAG, Visai, L, Valtulina, V, Schwarz-Linek, U, Norris, NC, Gurusiddappa, S, Höök, M, Speziale, P, & Potts, JR. (2007) *J. Biol. Chem.* **282**, 25893-25902
11. Kim, JH, Singvall, J, Schwarz-Linek, U, Johnson, BJB, Potts, JR, & Höök, M. (2004) *J. Biol. Chem.* **279**, 41706-41714
12. Tucker, RP, & Chiquet-Ehrismann, R. (2009) *Int. J. Biochem. Cell Biol.* **41**, 424-434
13. George, EL, Georges-Labouesse, EN, Patel-King, RS, Rayburn, H, & Hynes, RO. (1993) *Development* **119**, 1079-1091
14. Watt, FM, & Hodivala, KJ. (1994) *Curr. Biol.* **4**, 270-272
15. Magnusson, MK, & Mosher, DF. (1998) *Arterioscler. Thromb. Vasc. Biol.* **18**, 1363-1370
16. DeSimone, DW, Norton, PA, & Hynes, RO. (1992) *Dev. Biol.* **149**, 357-369
17. Cunningham, MW. (2000) *Clin. Microbiol. Rev.* **13**, 470-511
18. Rohde, M, Muller, E, Chhatwal, GS, & Talay, SR. (2003) *Cell. Microbiol.* **5**, 323-342
19. Molinari, G, Talay, SR, Valentin-Weigand, P, Rohde, M, & Chhatwal, GS. (1997) *Infect. Immun.* **65**, 1357-1363
20. Ozeri, V, Rosenshine, I, Mosher, DF, Fässler, R, & Hanski, E. (1998) *Mol. Microbiol.* **30**, 625-637
21. Nitsche-Schmitz, DP, Rohde, M, & Chhatwal, GS. (2007) *Thromb. Haemost.* **98**, 488-496
22. Schwarz-Linek, U, Höök, M, & Potts, JR. (2006) *Microb. Infect.* **8**, 2291-2298
23. Mosher, DF. (2006) *Arterioscler. Thromb. Vasc. Biol.* **26**, 1193-1195
24. Penkett, CJ, Dobson, CM, Smith, LJ, Bright, JR, Pickford, AR, Campbell, ID, & Potts, JR. (2000) *Biochemistry* **39**, 2887-2893
25. Bingham, RJ, Rudino-Pinera, E, Meenan, NAG, Schwarz-Linek, U, Turkenburg, JP, Höök, M, Garman, EF, & Potts, JR. (2008) *Proc. Natl Acad. Sci.* **105**, 12254-12258
26. Clackson, T, & Wells, JA. (1995) *Science* **267**, 383-386
27. Bogan, AA, & Thorn, KS. (1998) *J. Mol. Biol.* **280**, 1-9
28. Arkin, MR, & Wells, JA. (2004) *Nat. Rev. Drug Discov.* **3**, 301-317
29. Tuncbag, N, Keskin, O, & Gursoy, A. *Nucleic Acids Res.* **38**, W402-W406
30. Darnell, SJ, Page, D, & Mitchell, JC. (2007) *Proteins: Structure, Function, and Bioinformatics* **68**, 813-823
31. Kortemme, T, Kim, DE, & Baker, D. (2004) *Sci. STKE* **2004**, pl2-
32. Mészáros, B, Tompa, P, Simon, I, & Dosztányi, Z. (2007) *J. Mol. Biol.* **372**, 549-561
33. Bright, JR, Pickford, AR, Potts, JR, & Campbell, ID. (2000) *Methods Mol. Biol.* **139**, 59-69
34. Pope, B, & Kent, HM. (1996) *Nucl. Acids Res.* **24**, 536-537
35. Delaglio, F, Grzesiek, S, Vuister, GW, Zhu, G, Pfeifer, J, & Bax, A. (1995) *J. Biol. NMR* **6**, 277-293
36. Vranken, WF, Boucher, W, Stevens, TJ, Fogh, RH, Pajon, A, Llinas, M, Ulrich, EL, Markley, JL, Ionides, J, & Laue, ED. (2005) *Proteins: Struct. Funct. Bioinform.* **59**, 687-696
37. Marsh, JA, Singh, VK, Jia, Z, & Forman-Kay, JD. (2006) *Protein Sci.* **15**, 2795-2804

38. Wang, Y, & Jardetzky, O. (2002) *J. Am. Chem. Soc.* **124**, 14075-14084
39. Leslie, AGW. (1992) *Jnt CCP4/ESF-EACBM Newsl. Protein Crystallogr.* **26**, Daresbury Laboratory, Warrington, U.K.
40. Evans, P. (2006) *Acta Crystallogr. D Biol. Crystallogr.* **62**, 72-82
41. Collaborative Computational Project. (1994) *Acta Crystallogr D Biol Crystallogr.* **50**, 760-763
42. McCoy, AJ, Grosse-Kunstleve, RW, Adams, PD, Winn, MD, Storoni, LC, & Read, RJ. (2007) *J. Appl. Crystallog.* **40**, 658-674
43. Murshudov, GN, Vagin, AA, & Dodson, EJ. (1997) *Acta Crystallogr. D Biol. Crystallogr.* **53**, 240-255
44. Eddy, SR. (1998) *Bioinformatics* **14**, 755-763
45. Suzek, BE, Huang, H, McGarvey, P, Mazumder, R, & Wu, CH. (2007) *Bioinformatics* **23**, 1282-1288
46. Schuster-Bockler, B, Schultz, J, & Rahmann, S. (2004) *BMC Bioinformatics* **5**, 7
47. Sali, A, & Blundell, T. (1993) *J. Mol. Biol.* **234**, 779-815
48. House-Pompeo, K, Xu, Y, Joh, D, Speziale, P, & Höök, M. (1996) *J. Biol. Chem.* **271**, 1379-1384
49. Hutchinson, EG, Sessions, RB, Thornton, JM, & Woolfson, DN. (1998) *Prot. Sci.* **7**, 2287-2300
50. Saha, RP, Bahadur, RP, Pal, A, Mandal, S, & Chakrabarti, P. (2006) *BMC Struct. Biol.* **6**, 11
51. Lo Conte, L, Chothia, C, & Janin, J. (1999) *J. Mol. Biol.* **285**, 2177-2198
52. Chakrabarti, P, & Janin, J. (2002) *Proteins: Struct. Funct. Genetics* **47**, 334-343
53. Gunasekaran, K, Tsai, CJ, Kumar, S, Zanuy, D, & Nussinov, R. (2003) *Trends Biochem. Sci.* **28**, 81-85
54. Deane, JE, Ryan, DP, Sunde, M, Maher, MJ, Guss, JM, Visvader, JE, & Matthews, JM. (2004) *EMBO J.* **23**, 3589-3598
55. Fuxreiter, M, Simon, I, Friedrich, P, & Tompa, P. (2004) *J. Mol. Biol.* **338**, 1015-1026
56. Schreiber, G, & Fersht, AR. (1995) *J. Mol. Biol.* **248**, 478-486
57. Wells, JA, & de Vos, AM. (1993) *Annu. Rev. Biophys. Biomol. Struct.* **22**, 329-351
58. Janin, J, Bahadur, RP, & Chakrabarti, P. (2008) *Quart. Rev. Biophys.* **41**, 133-180
59. Tuncbag, N, Gursoy, A, & Keskin, O. (2009) *Bioinformatics* **25**, 1513-1520
60. Vakonakis, I, Staunton, D, Ellis, IR, Sarkies, P, Flanagan, A, Schor, AM, Schor, SL, & Campbell, ID. (2009) *J. Biol. Chem.* **284**, 15668-15675
61. Radivojac, P, Iakoucheva, LM, Oldfield, CJ, Obradovic, Z, Uversky, VN, & Dunker, AK. (2007) *Biophys. J.* **92**, 1439 - 1456
62. Dosztányi, Z, Csizmók, V, Tompa, P, & Simon, I. (2005) *J. Mol. Biol.* **347**, 827-839
63. Dunker, AK, & Uversky, VN. (2010) *Curr. Opin. Pharmacol.* **10**, 782-788
64. Bahadur, RP, Chakrabarti, P, Rodier, F, & Janin, J. (2004) *J. Mol. Biol.* **336**, 943-955

TABLE 1
Thermodynamic parameters for the interaction between pNTD and SfbI-5 mutants determined by ITC at 37°C, pH 7.4

SfbI-5 or SfbI-5 mutant	K_d (nM)	ΔH° (kcal/mol)	ΔS° (cal mol^{-1} K^{-1})	ΔG° (kcal/mol)	ΔΔG° (kcal/mol)
SfbI-5	3.5 ± 0.2	−45.4 ± 0.7	−108	−11.99 ± 0.04	0.00 ± 0.06
V552A	10.6 ± 0.8	−44.3 ± 0.2	−106	−11.30 ± 0.05	0.69 ± 0.06
E553A	8.4 ± 0.8	−45.2 ± 0.3	−109	−11.45 ± 0.06	0.54 ± 0.08
F554A	31.5 ± 4.9	−42.9 ± 0.7	−104	−10.63 ± 0.10	1.36 ± 0.10
K556A	1.6 ± 0.2	−45.7 ± 1.4	−107	−12.46 ± 0.08	−0.47 ± 0.09
K556E	0.8 ± 0.2	−49.0 ± 2.4	−116	−12.90 ± 0.18	−0.90 ± 0.18
D557A	13.8 ± 1.0	−43.2 ± 0.2	−103	−11.14 ± 0.05	0.85 ± 0.06
T558A	55.4 ± 2.7	−37.9 ± 1.6	−89.0	−10.29 ± 0.03	1.70 ± 0.05
M562A	8.2 ± 0.4	−40.0 ± 0.1	−92.2	−11.46 ± 0.03	0.53 ± 0.05
G564A	28.7 ± 2.1	−38.5 ± 0.2	−89.6	−10.69 ± 0.04	1.30 ± 0.06
I571A	7.7 ± 0.3	−44.5 ± 0.1	−106	−11.50 ± 0.03	0.49 ± 0.05
E573A	13.9 ± 0.8	−43.6 ± 0.2	−105	−11.14 ± 0.03	0.85 ± 0.06
D574A	41.0 ± 5.9	−46.3 ± 1.2	−116	−10.47 ± 0.09	1.52 ± 0.10
T575A	11.1 ± 0.5	−44.9 ± 0.4	−108	−11.27 ± 0.03	0.72 ± 0.05

TABLE 2
Analysis of the interfaces in the $^{2}F1^{3}F1$:PyTT5 complex by change in ASA on complex formation.

Complex	**$^{2}F1^{3}F1$:PyTT5**		
Molecule, chain	$^{2}F1^{3}F1$, B	PyTT5, D	Complex
Interface area (Å^{2})			
Total	851.4	1095.6	1947.0
Core	653.1	853.0	1506.1
Rim	241.5	242.6	484.1
Interface area / Surface area	0.17	0.41	0.24
Number of interface atoms			
Total	122	89	211
Buried	44	22	66
Accessible	78	67	145
Number of interface residues			
Total	38	18	56
Core	20	14	34
Rim	18	4	22
Fraction of non-polar atoms	0.57	0.60	0.58
Non-polar interface area (Å^{2})	443.5	592.3	1035.8
Fraction of fully buried atoms	0.36	0.25	0.31
Local Density	36.56	32.70	

Statistics for the interface between $^{2}F1^{3}F1$ chain B and PyTT5 chain D were calculated with the ProFace server (50). Local density is a measure of the atomic packing at the interface (64).

TABLE 3
Parameters for the interaction of pNTD and Fn with SfbI-5 and the T558A mutant determined using SPR at 25°C, pH 7.4

Construct	k_1[a] ($\times 10^7$ M^{-1} s^{-1})	k_{-1}[a] ($\times 10^{-4}$ s^{-1})	K_d (nM)	ΔG° (kcal/mol)	ΔΔG° (kcal/mol)
pNTD					
SfbI-5	2.89	39.7	0.137 ± 0.002	−13.44 ± 0.01	0.00
T558A	n/d[b]	n/d[b]	2.6 ± 0.3	−11.71 ± 0.07	1.74 ± 0.07
Fn					
SfbI-5	0.462	1.405	0.030 ± 0.001	−14.35 ± 0.00	0.00
T558A	0.170	2.33	0.137 ± 0.004	−13.44 ± 0.02	0.91 ± 0.02

[a] For each experiment, the errors for k_1, k_{-1} and K_d were calculated from the errors in fitting the data from a single kinetic series to a Langmuir 1:1 binding model . The fitting model minimizes the errors associated with each variable. For all experiments, the errors for k_1 and k_{-1} came out to zero when expressed to a suitable number of significant figures.
[b] n/d, not determined. The data obtained for T558A:pNTD did not fit a kinetic model and was, therefore, fitted to a steady state affinity model. Thus, there is no kinetic data available for this experiment.

FIGURE 1.

SfbI-5 is intrinsically disordered. *A,* The ^{1}H, ^{15}N HSQC spectrum of ^{15}N, ^{13}C-labelled SfbI-5. The peaks in the spectra were assigned to the $^{1}H^{N}$ and ^{15}N resonances of SfbI-5 residues using standard procedures. Each peak is labelled according to its position in the full-length SfbI-5 sequence. The peak annotated I(540) is not native to full-length SfbI, but is directly N-terminal to P541 from native SfbI, and the peak annotated R576 is from the side-chain of R576. The other smaller, unassigned peaks in close proximity to assigned resonances are likely to arise from residues near a proline as a result of the proline being in a *cis*-conformation. Inset is an enlarged area of the boxed region of the spectrum. *B,* The sequence-corrected SSP score was calculated for SfbI-5 using all available chemical shift information. SSP scores of +1 and −1 represent a stable α-helix and β-strand, respectively. A score of 0 represents random coil.

FIGURE 2.

Conserved FnBR residues identified with an iterative HMM search of the UniRef90 database. Shown above the HMM logo are *A,* the crystal structures of ^{2}F1^{3}F1 and ^{4}F1^{5}F1 (purple) bound to FnBPA-1 peptides (grey) shown in ribbon representation (23,25). Conserved FnBPA-1 and F1-module side-chains important in the interaction are shown in stick representation and are coloured yellow or cyan, respectively. Hydrogen bonds are shown as black dashed lines and two bridging water molecules as grey spheres. *B*, the sequences of FnBPA-1 (residues 476-514) and the SfbI-5 $^{2-5}$F1 binding region (residues 544–578) are aligned to the columns in the HMM logo. Conserved FnBPA-1 side-chains are also highlighted yellow in the FnBPA-1 sequence, and SfbI-5 residues chosen for mutation to alanine are highlighted green. The SfbI-5 residue K556 is underlined: this residue was also mutated separately to glutamate. Regions of FnBPA-1 that form a β-strand when bound to F1 modules are indicated above the sequences by grey arrows. The logo was drawn with the LogoMat-M server, www.sanger.ac.uk/Software/analysis/logomat-m/.

FIGURE 3.

ITC studies of SfbI-5 (wild-type and mutants) binding to pNTD. *A*, wild-type, *B*, K556E, *C*, K556A, *D*, M562A, *E*, E553A and *F*, T558A. In each sub-figure, the top panel shows the experimental trace as a solution of SfbI-5 (or SfbI-5 mutant) was titrated into a pNTD solution. When a control titration was used to account for heats of dilution it is also shown, but displaced by −0.03 µcal/s. The bottom panel shows the processed molar heats of binding normalized to the ratio between SfbI-5 (or SfbI-5 mutant) to pNTD. For each titration, the curve from non-linear least squares regression analysis, using a single-site binding model is shown in grey. Thermodynamic parameters derived from these experiments are in Table 1.

FIGURE 4.

Structure of ^{2}F1^{3}F1:PyTT5 PyTT5 (green) binds along the E strands of both modules in ^{2}F1^{3}F1 (purple). *A,* One of the two ^{2}F1^{3}F1:PyTT5 complexes in the asymmetric unit. . *B,* ^{2}F1^{3}F1:PyTT5 structure showing the difference density at a level of 1 sigma (grey) when the PyTT5 molecule is deleted. *C,* The interaction between ^{2}F1^{3}F1 and the ^{3}F1-binding and linker regions of PyTT5 shown as a stick representation *D,* The interaction between ^{2}F1 and the ^{2}F1-binding region of PyTT5 shown as a stick representation. In both *C* and *D,* hydrogen bonds and salt-bridges are black dashes and invariant bridging water molecules are shown as grey spheres. Residues mentioned in the text are labelled.

FIGURE 5.

The interface between ^{2}F1^{3}F1 and PyTT5. Surface representation of ^{2}F1^{3}F1 and PyTT5 (left and right, respectively) showing the interface between ^{2}F1^{3}F1 and PyTT5. Indicated are the ^{2}F1 and ^{3}F1 modules, as are the regions of PyTT5 that bind ^{2}F1and ^{3}F1. The schematic above the interfaces shows how the complex was opened like a book to reveal the interface. *A,* The interface is shown at the atom

level and is represented as buried and accessible atoms, which are coloured red and blue, respectively. *B,* The interface is shown at the residue level and is represented as core (magenta) and rim (cyan) residues. Residue and atom accessibility was calculated from the output of ProFace (50).

FIGURE 6.

Model of the $^{1-5}$F1:SfbI-5 complex. Ribbon representation of a model of SfbI-5 (green) in complex with $^{1-5}$F1 (purple).

FIGURE 7.

SPR studies of GST-SfbI-5 (wild-type and T558A) binding to Fn. Either *A*, GST-SfbI-5 or *B*, SfbI-5 T558A was immobilised on the chip. Dimeric plasma Fn or pNTD was used as the analyte. SPR response curves, baseline corrected, are shown in black; and the best-fits to the data of Langmuir 1:1 models are shown in grey. Parameters derived from these experiments are shown in Table 3.

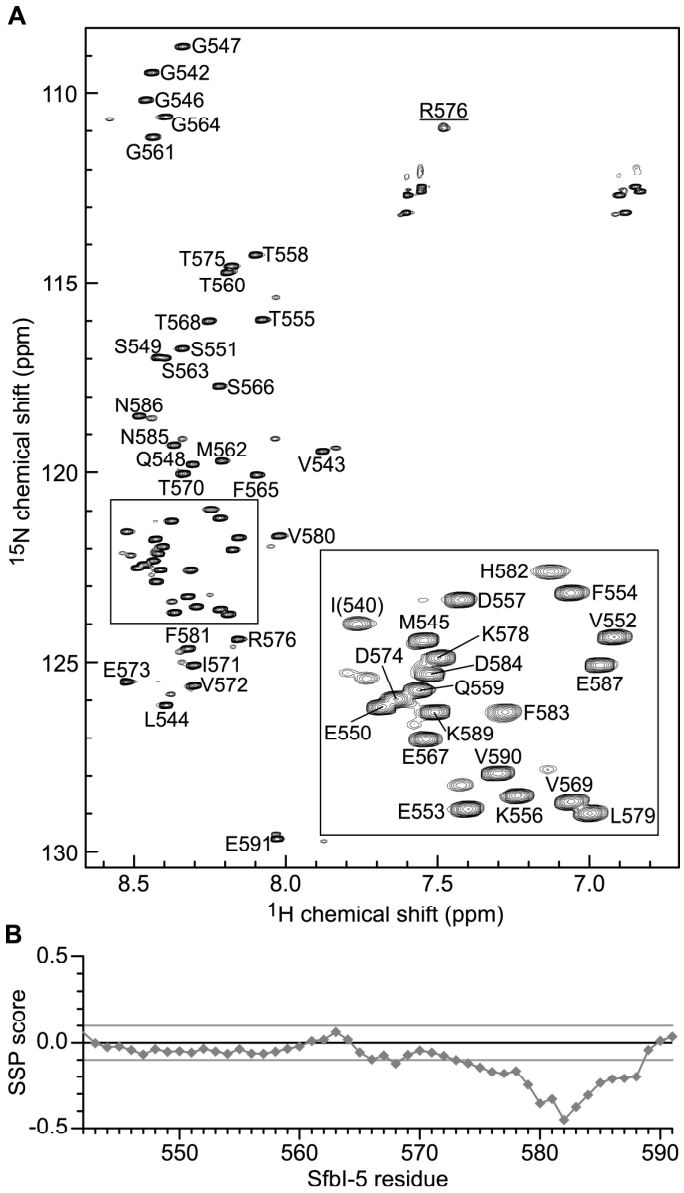
A
G547
G542
G546
G564
G561
R576
T575
T558
T560
T568
T555
S549
S551
S563
S566
N586
N585
M562
Q548
V543
T570
F565
V580
F581
R576
E573
I571
V572
L544
E591
H582
D557
F554
I(540)
M545
V552
K578
D574
D584
Q559
E587
F583
E550
K589
E567
V590
V569
E553
K556
L579
110
115
120
125
130
8.5
8.0
7.5
7.0
15N chemical shift (ppm)
1H chemical shift (ppm)
B
0.5
0.0
-0.5
SSP score
550
560
570
580
590
Sfbl-5 residue

Figure 1

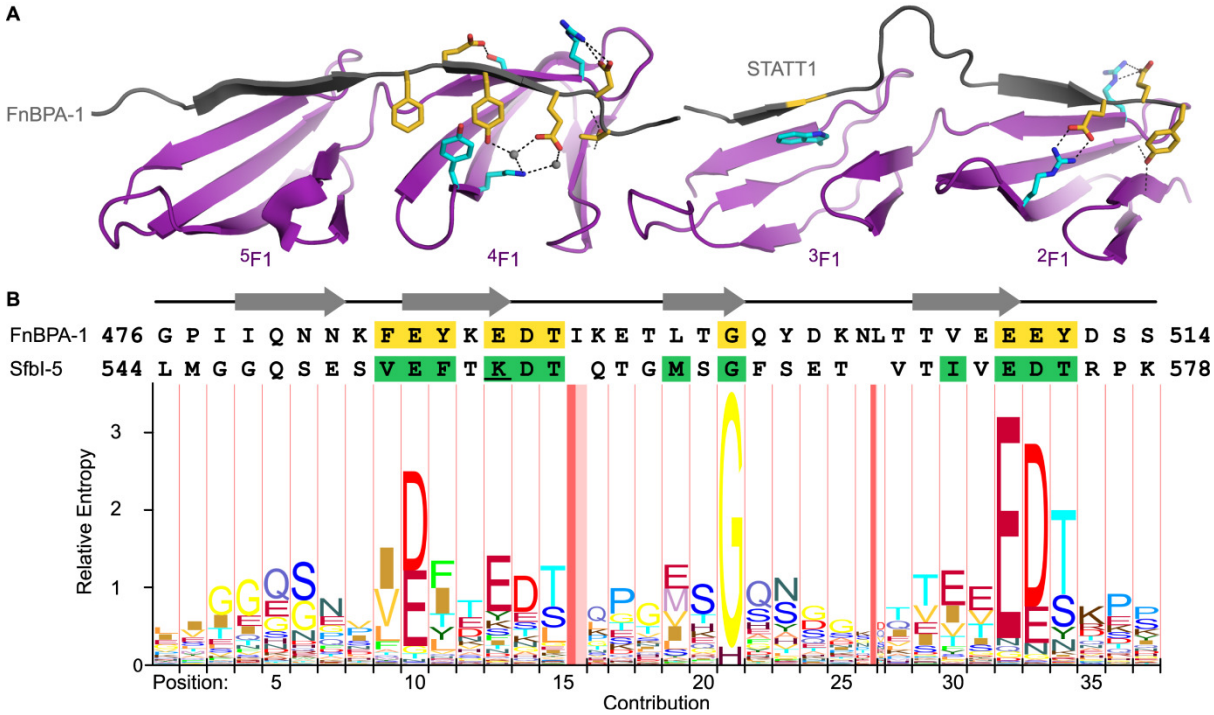
A
FnBPA-1
STATT1
5F1
4F1
3F1
2F1
B
FnBPA-1 476 G P I I Q N N K F E Y K E D T I K E T L T G Q Y D K N L T T V E E E Y D S S 514
SfbI-5 544 L M G G Q S E S V E F T K D T Q T G M S G F S E T V T I V E D T R P K 578
Relative Entropy
Position:
Contribution

Figure 2

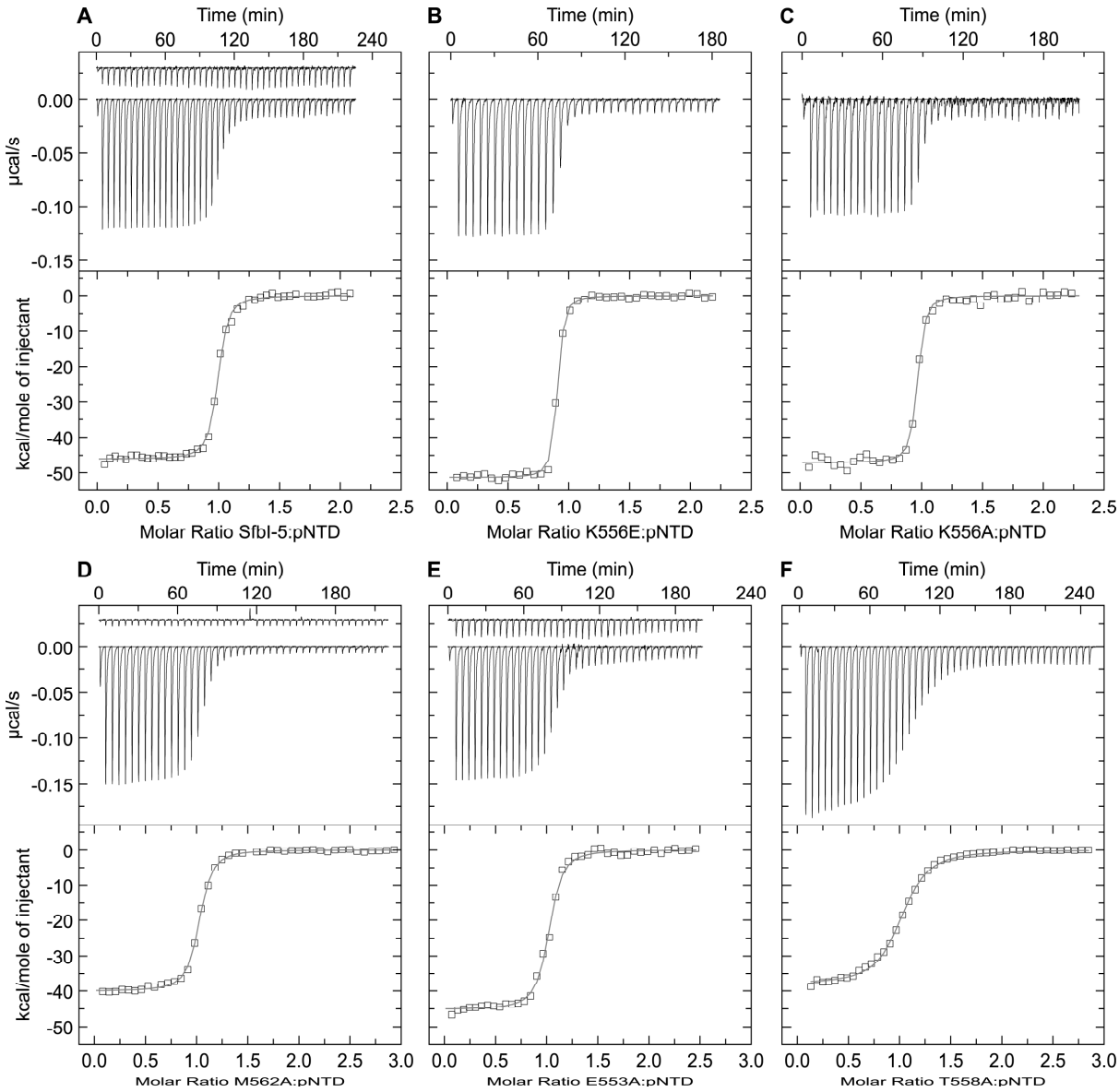
A
Time (min)
0
60
120
180
240
µcal/s
0.00
-0.05
-0.10
-0.15
kcal/mole of injectant
0
-10
-20
-30
-40
-50
0.0
0.5
1.0
1.5
2.0
2.5
Molar Ratio SfbI-5:pNTD
B
Time (min)
Molar Ratio K556E:pNTD
C
Time (min)
Molar Ratio K556A:pNTD
D
Time (min)
3.0
Molar Ratio M562A:pNTD
E
Time (min)
Molar Ratio E553A:pNTD
F
Time (min)
Molar Ratio T558A:pNTD

Figure 3

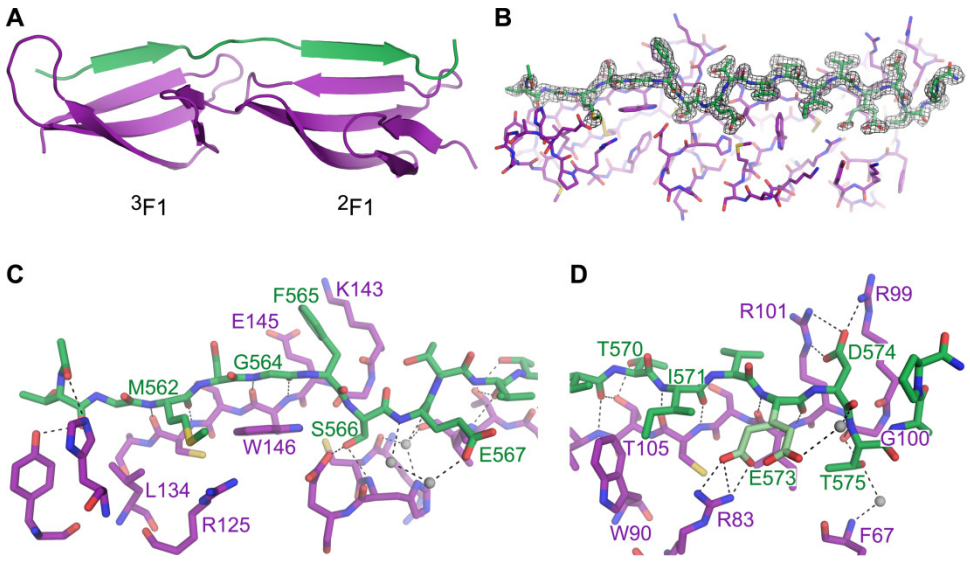

Figure 4

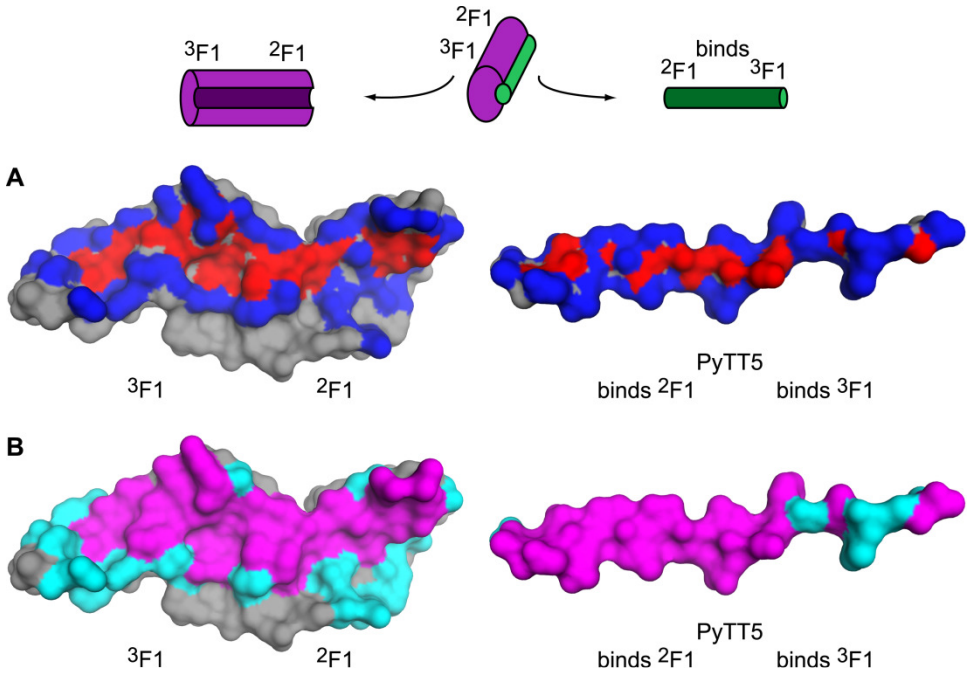

Figure 5

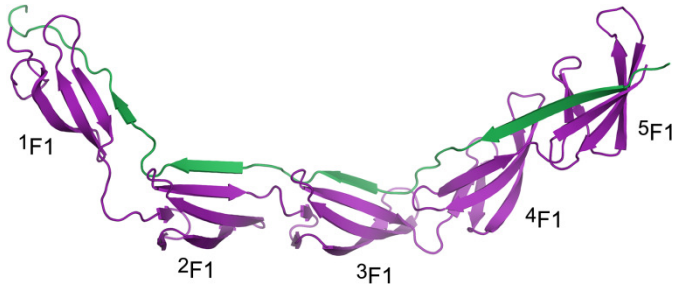

Figure 6

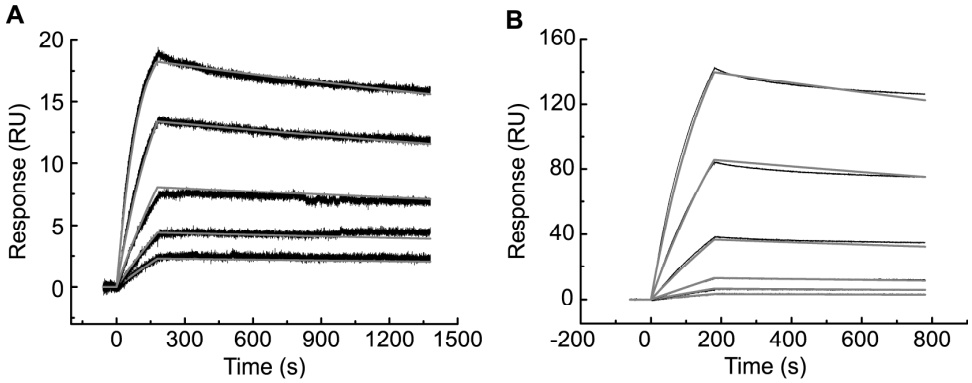

Figure 7